D. Zagaglia, A. Zanotti, G. Gibertini
Analysis of the Loads Acting on the Rotor of a Helicopter Model Close to an Obstacle in Moderate Windy Conditions
Aerospace Science and Technology, Vol. 78, 2018, p. 580-592
doi:10.1016/j.ast.2018.05.019

Analysis of the loads acting on the rotor of a helicopter model close to an obstacle in moderate windy conditions

D. Zagaglia[1,*], A. Zanotti[1], G. Gibertini[1]

Politecnico di Milano, Dipartimento di Scienze e Tecnologie Aerospaziali
Campus Bovisa, Via La Masa 34, 20156 Milano, Italy

Abstract

The present paper describes an experimental investigation of the loads acting on a rotor when it interacts with a simplified cuboid obstacle, representing a low-rise building, in moderate windy conditions. Measurements of forces and moments acting on the rotor were carried out by means of a six-component balance in order to assess the rotor performance for several helicopter positions with respect to the obstacle. Wind tunnel tests have been carried out at an advance ratio of $\mu = 0.05$ and compared with the corresponding wind-off tests. The investigation showed that ground effect on the obstacle is generally mitigated in windy conditions and that severe detrimental effects are encountered when the helicopter enters the obstacle wake, especially when the helicopter interacts with its lateral vortex structures.

Keywords: Helicopter, Interactional Aerodynamics, Ground Obstacles, Rotor Loads, Ground Effect, Wind Tunnel

*Corresponding author
Email address: daniele.zagaglia@polimi.it (D. Zagaglia)

Nomenclature

A	=	Rotor disk area, πR^2, m^2
c	=	Blade chord, m
c_∞	=	Asymptotic speed of sound, m/s
c_{Mx}, c_{My}	=	Rotor in-plane moment coefficients, $M/(\rho V_{TIP}^2 AR)$, –
c_Q	=	Rotor torque coefficient, $Q/(\rho V_{TIP}^2 AR)$, –
c_T	=	Rotor thrust coefficient, $T/(\rho V_{TIP}^2 A)$, –
D	=	Rotor diameter, m
FM	=	Figure of Merit, $C_T^{3/2}/(C_Q\sqrt{2})$, –
M_{TIP}	=	Mach number at blade tip, V_{TIP}/c_∞, –
M_x, M_y	=	Rotor in-plane moments, Nm
Q	=	Rotor torque, Nm
R	=	Rotor radius, m
Re_{TIP}	=	Reynolds number at blade tip, $V_{TIP}c/\nu$, –
T	=	Rotor thrust, N
U_∞	=	Free-stream velocity, m/s
V_{TIP}	=	Blade tip velocity, ΩR, m/s
(X, Y, Z)	=	Absolute reference system
(x, y, z)	=	Rotor reference system
ν	=	Fluid cinematic viscosity, m^2/s
ρ	=	Air density, kg/m^3
ϵ_{c_T}	=	Uncertainty on the Thrust coefficient, –
ϵ_{FM}	=	Uncertainty on the Figure of Merit, –
μ	=	Advance ratio, U_∞/V_{TIP}, –
Ω	=	Rotational frequency of the rotor, RPM

1. Introduction

The helicopter is a very versatile flying machine which, thanks to its peculiar capability of managing hovering flight, is often required to operate within confined areas. Naval operations, e.g. the landing manoeuvre on a helicopter carrier, and rescue operations in confined areas, such as close to buildings and mountain walls, are typical operative conditions where the helicopter is forced to interact with the surroundings.

This aerodynamic interference between the rotor-induced wake and the surrounding obstacles typically generates a degradation of the helicopter performance and a high compensatory workload for the pilot [1]. In particular these helicopter/obstacle aerodynamic interactions can cause recirculating flows due to the deflection of the rotor-induced downwash, which can potentially lead to hazardous flight situations. These flight conditions can cause rapid trim changes leading to aircraft control difficulties, and potentially, collision with the obstacle itself. This situation can be further complicated by the presence of wind, since the helicopter has to interact with the complex, highly unsteady and turbulent wake generated by the obstacle.

Timm [2] was the first to observe the flow recirculation induced by the interaction between the rotor and obstacle through flow visualisations. More recently, the ground effect of a fully articulated rotor above a confined area between two vertical walls was investigated by Iboshi et al., [3].

The Dynamic Interface problem [4], i.e. the launch and recovery of flight vehicles, primarily rotorcraft, onto ships in windy conditions is probably the most investigated configuration from both the experimental and numerical point of view. Zan [5] produced one of the first experimental works on this topic, presenting the measurements of time-averaged rotor thrust coefficients for a rotor immersed in the airwake of the Canadian Patrol Frigate ship. This work shows how the interaction can significantly decrease rotor thrust up to 15%, thereby impacting operational envelopes. Zan proposed a set of changes in the ship superstructure geometry which were able to reduce the severity of the airwake and also lessen the spatial gradients of the rotor thrust coefficient. Further studies allowed to investigate also the

unsteady loads on the fuselage immersed in the ship wake [6] and the full configuration comprising rotor and fuselage [7].

Other test rigs have been developed for the study of a helicopter in the airwake of a ship, like the one by Kääriä et al. [8; 9]. In particular experiments were conducted in a water tunnel using a specially designed Airwake Dynamometer (AirDyn) to characterise the aerodynamic loading of the helicopter immersed in the ship-wake, showing very strong variation of both average and unsteady loads due to the strong velocity gradients that develop in the wake of the ship.

The flow that is generated in the helicopter/obstacle interaction has been investigated as well. As an example, Quinliven and Long [10] investigated the inflow region and the wake of a rotor in proximity of a building model, highlighting the effect of the flow-recirculation that occurs when the rotor is close to the building. Particle Image Velocimetry (PIV) was used by Rajagopalan et al. [11] to acquire 3-component velocity field measurements of the combined wake of a tandem-rotor helicopter and a ship. PIV was also used by Nacakli and Landman [12] to investigate the recirculation region between a rotor and the vertical wall of a ship deck. Measurements of the downwash and outwash from the rotor of a full-scale helicopter hovering near a land-based hangar were achieved by Polsky and Wilkinson [13].

Despite the presence of a fair number of numerical and experimental investigations, a systematic study of these aerodynamic phenomena is still lacking. Moreover the past studies usually involve very specific geometries (e.g. ship decks, specific buildings).

The idea behind the present work is thus to experimentally investigate this problem, simplifying the obstacle geometry up to a well-defined parallelepiped shape in order to disclose the key fluid-dynamic mechanisms that occur when a helicopter is hovering in its proximity. Similarly, a rigid unarticulated rotor was adopted, not allowing the flapping and lag blade motion which are quite difficult to be monitored on a small-scale model. In this way, the rotor geometry was *a priori* known and well-defined. Due to this choice, this very rigid hinge-less rotor with fixed pitch angle was untrimmed for helicopter equilibrium (also without the obstacle) and therefore it did not reproduce the dynamics of a real helicopter rotor. Nevertheless, the general features of its wake were still representative of those of a real

one, thus the observed phenomena are not expected to be excessively affected by this choice. In the present work, the results will be referred to the corresponding (with or without wind) out of ground effect (OGE) condition, in order to identify the combined effect of both the ground and the obstacle and give an indication of the required pilot correction in a real case.

The aerodynamic behaviour of a complete, real helicopter is obviously very complex, due to the contribution of its different components such as the fuselage, the main rotor and the tail rotor, which interact with each other. A better understanding of each contribution can be obtained analysing separately their influence, thus generalising the observations and giving useful information for the development of flight control systems or simulation tools to be included in flight simulators. In light of these considerations, the present study was focused on the main rotor only. The tail rotor was not included in the model while a simple fuselage was present in order to create a more realistic rotor wake and shield the main model frame, which held the balance, the motor and its controller.

A first experiment [14] was initially carried out at Politecnico di Milano, analysing the case of a model helicopter with fuselage interacting with a cuboid obstacle in absence of wind. Subsequently, the present work intends to investigate how the phenomena that were observed in absence of external wind are affected by a moderate wind that flows past the obstacle.

To do so, a new test campaign was carried out in the framework of the GARTEUR AG22 action group [15], consisting in the analysis of a helicopter model interacting with a parallelepiped-shaped obstacle in both windy and not-windy conditions. Load measurements on the rotor were carried out in order to monitor the variations in the rotor performance for several helicopter model positions with respect to the obstacle. An additional database, analysing the interaction of a rotor without fuselage in absence of wind, was obtained at the University of Glasgow [16] in the framework of GARTEUR AG22 as well. The obtained databases are available on request so that they can be also used for the assessment of Computation Fluid Dynamics (CFD) codes as it has already been done, for instance, by Chirico et al. [17] with the previous test campaign of [14].

2. Experimental setup and test points

2.1. Experimental setup

The test rig that was used during the test campaign at Politecnico di Milano essentially consisted of a helicopter model and a parallelepiped obstacle which represented an ideal building, as represented in Figure 1. The helicopter model was held by a horizontal strut fixed to a system of two motorised orthogonal sliding guides to allow the relative position to be changed with respect to the obstacle along the vertical and longitudinal directions of the fuselage. Two different reference systems are defined, as represented in Figure 2. The global reference system (X, Y, Z) defines the position of the rotor hub centre with respect to the obstacle, whereas the rotor reference system (x, y, z) was used to define the force and moment components acting on the rotor. The origin of the absolute (X, Y, Z) coordinate system is fixed and it is placed on the floor, at the obstacle mid-span, so that the X-coordinate represents the distance of the rotor centre from the obstacle, the Y-coordinate represents the distance of the rotor centre from symmetry plane and the Z-coordinate represents the height of the rotor centre from the ground. Therefore the X-Z lies in the mid-span plane of the building model and the X-Y plane is coincident with the floor. The X coordinate grows as the helicopter is positioned further from the obstacle, the Y coordinate as the helicopter is positioned to the right of the obstacle and the Z coordinate as the helicopter is positioned upwards.

The tests were carried out in the large test chamber, suitable for wind engineering tests, of the Large wind tunnel of Politecnico di Milano (GVPM, see Reference [18]), as depicted in Figure 3. The test chamber is 13.84 m wide, 3.84 m high and 38 m long. Despite the huge test chamber, a relatively small model was used so that the interference effect with the surrounding walls could be considered negligible. A schematic of the rotor and obstacle models inside the test chamber is depicted in Figure 4.

The rotor had four untwisted and untapered rectangular blades, using the NACA 0012 airfoil. No swash plate was present, so the blade pitch angle was fixed to 10°. The direction of rotation was counter-clockwise when seen from above, as represented in Figure 2. A

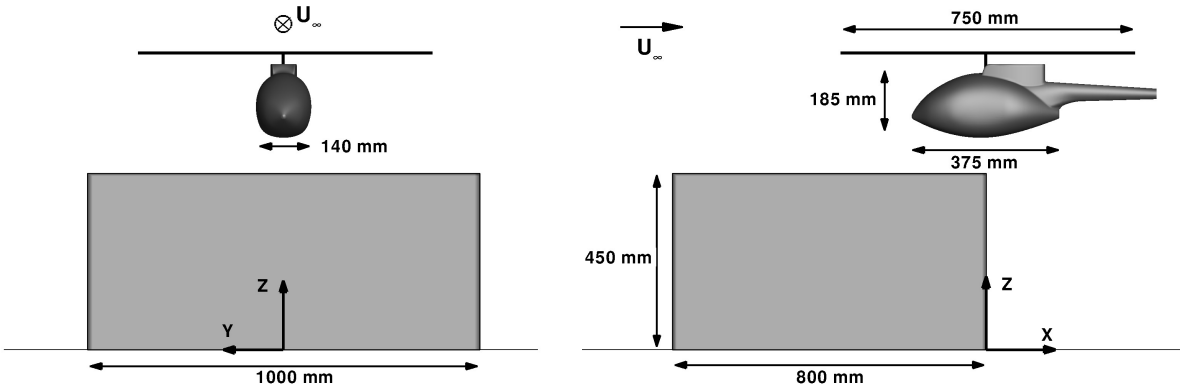

(a) Test Rig - Frontal View

(b) Test Rig - Lateral View

Figure 1: Schematic of the test rig geometry.

rotational speed of approximately 2580 RPM was maintained during all the tests by means of a brush-less low-voltage electrical motor with an electronic controller. The resulting Mach number and Reynolds number at the blade tip were $M_{\text{TIP}} = 0.30$ and $Re_{\text{TIP}} = 220,000$, respectively. The rotor rig features and the test operating condition are summed up in Table 1.

The limited Reynolds number implies a different resistant torque with respect to a full-scale condition, producing, to a certain extent, a different swirl of the rotor wake. The general rotor wake features are nevertheless expected to be representative of those of a real rotor. Moreover in the present investigation the employed model was able to reach a Reynolds number either similar or higher than most of the other in similar investigations (i.e. [10] and [11]).

The forces and moments acting on the rotor were measured with a six-component balance nested inside the fuselage. The schematic of the helicopter model is showed in Figure 5. The loads and moments will be expressed according to the rotor reference system (x, y, z) of Figure 2. Hence a positive M_y moment is equivalent to a pitching nose-up moment, and a positive M_x moment is equivalent to a roll moment that promotes a thrust rotation towards the positive y-coordinate. A Hall effect sensor produced one signal per revolution to act as the feedback signal for RPM control. According to the nominal accuracy of the whole

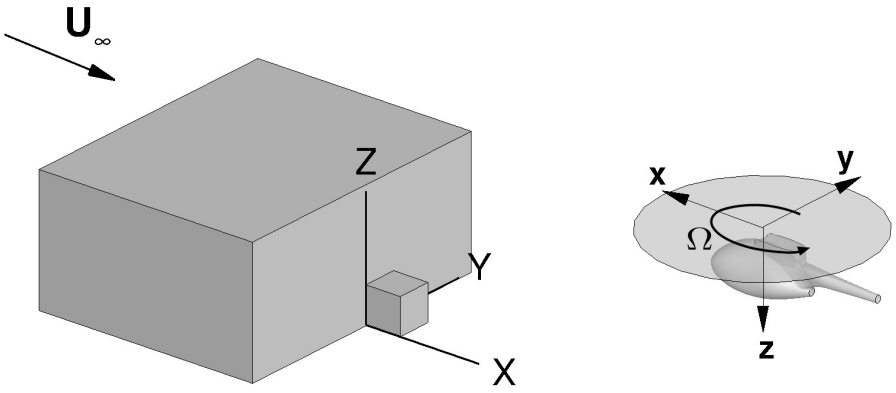

Figure 2: Schematic of the adopted absolute (X, Y, Z) and rotor (x, y, z) reference systems.

adopted instrumentation, the uncertainty on the measured thrust coefficient ϵ_{c_T} resulted to be 0.4 % of the Out of Ground Effect (OGE) value, while the uncertainty on the torque and pitch/roll moments resulted to be 0.48 % of the OGE torque coefficient. Combining the uncertainties on the thrust and the torque coefficients, the uncertainty on the Figure of Merit ϵ_{FM} resulted to be 0.76 % of the OGE value. A repeatability test over 30 realisations of the Out of Ground effect condition ($Z/R = 4$ in absence of the obstacle) exhibited a standard deviation of the thrust and torque coefficients equal to 0.31 % and 0.34 % respectively.

The obstacle model was a parallelepiped with sharp edges, comprising an internal structure of aluminium alloy square tubes that held the external aluminium alloy plates. The parallelepiped was 0.8 m long, 1 m wide and 0.45 m tall, thus representing the typical case of a wall-mounted cuboid obstacle. The flow around this kind of three-dimensional body has been widely studied in past investigations by means of both experiments ([19; 20; 21]) and numerical simulations ([20; 22; 23]). The features of the flow structures that develop around the wall-mounted obstacle are obviously dependent upon several parameters, such as the obstacle aspect ratio, the thickness of the inflow boundary layer with respect to the obstacle height, the Reynolds number, etc. However, if we just consider low-aspect ratio obstacles, the main flow structures that occur are mainly originated from the presence of the

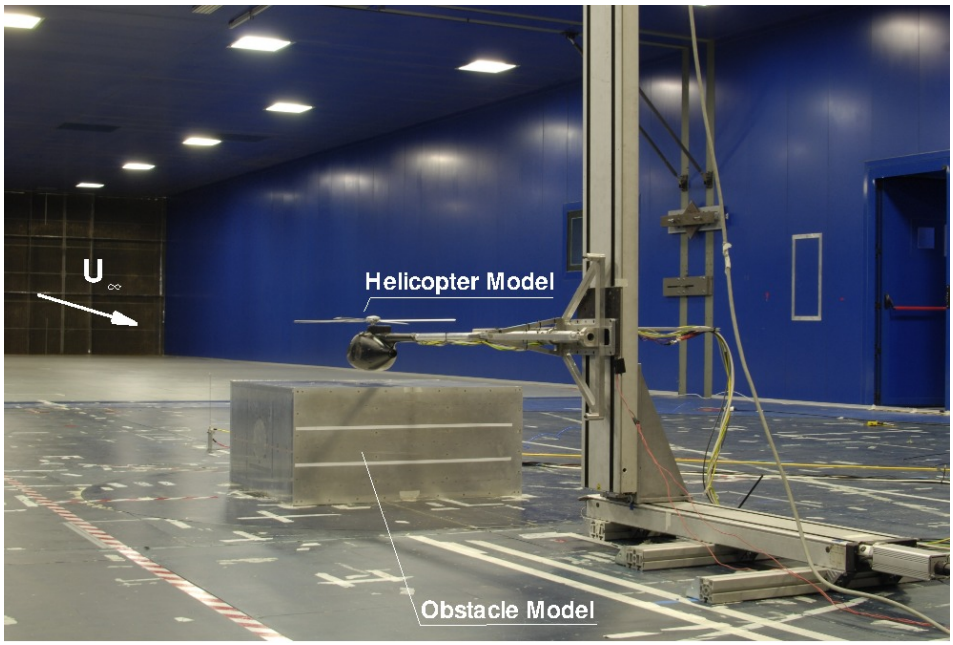

Figure 3: The rotor-obstacle test rig mounted inside the GVPM wind tunnel.

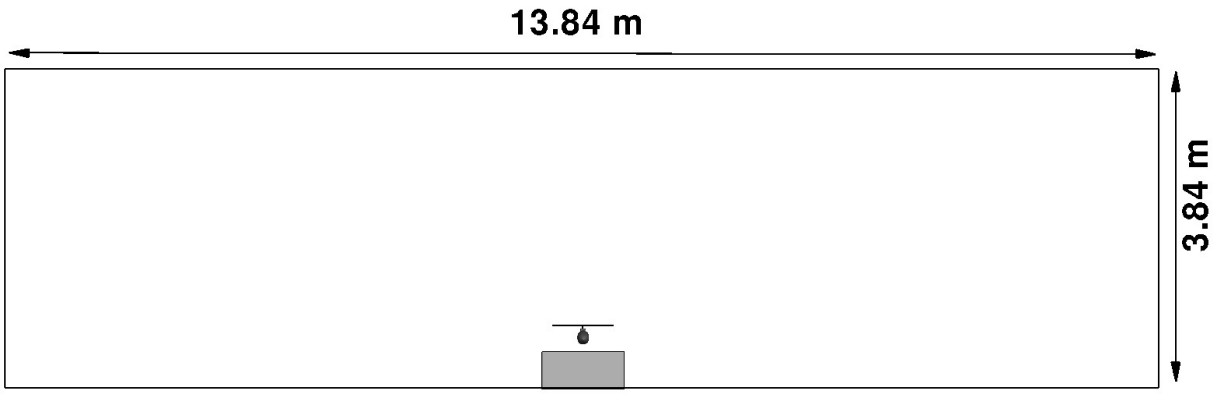

Figure 4: Schematic of the helicopter-obstacle test rig mounted inside the GVPM wind tunnel and test section dimensions.

Characteristics	
Obstacle size	1m × 0.8m × 0.45m (width/length/height)
Rotor Diameter	0.75 m
Number of blades	4
Blade chord	32 mm
Solidity	0.11
Collective pitch	10°
Rotor Rotational frequency	2580 RPM (43 Hz)
Reynolds Num. at blade tip	220000
Mach Num. at blade tip	0.30

Table 1: Main features of the test rig and operating conditions.

sharp edges. Thus their dimensions may change as function of the flow parameters, but the essence of the occurring phenomena is well-defined and scarcely influenced by the Reynolds number. A schematic of the average flow around a wall-mounted obstacle is presented in Figure 6, following Martinuzzi and Tropea [19]. The flow separation originates in the region upstream of the obstacle, usually at a distance approximately equal to the obstacle height. In particular, two main flow structures develop around the obstacle, if its aspect ratio (width/height) is sufficiently small: the horseshoe vortex that originates upstream of the obstacle, and an arch vortex just downstream of the obstacle.

The obstacle model was equipped with several pressure taps and the pressures were acquired contextually to the load measurements on the rotor. However the analysis of the loads on the obstacle model will not be addressed in the present paper, since the focus is on the change in the rotor performance. A few Particle Image Velocimetry surveys, carried out in a measurement window beside the obstacle downstream face, are not shown in the present paper as well since the PIV measurements were carried out just for T2, in a measurement window close to the ground and past the obstacle. Therefore, they do not contribute in a

significant way to the knowledge of the flow on the rotor disk.

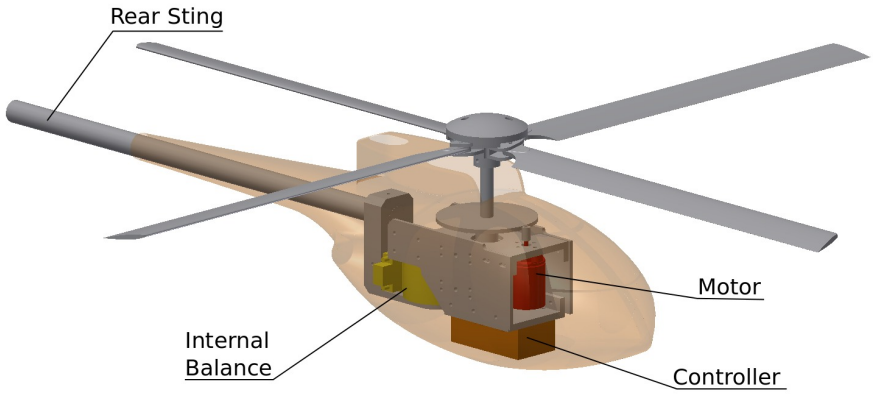

Figure 5: Layout of the helicopter model and nested instrumentation.

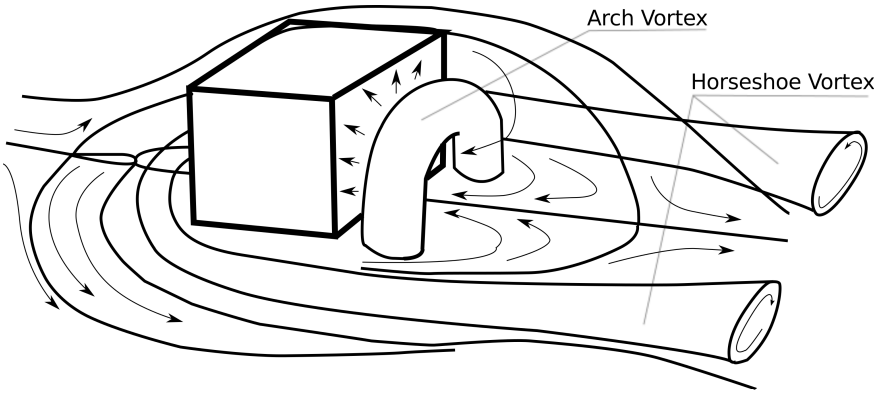

Figure 6: Schematic of the average flow around a low aspect-ratio, wall-mounted obstacle, according to Martinuzzi and Tropea[19]

2.2. Test points

Tests were carried out with the obstacle leaned on the 0.8 m $\times$ 1 m face to represent a low-rise building. With respect to the fixed reference system (X, Y, Z) shown in Figure 2, several series of tests consisting of vertical sweeps, where X and Y were constant, or horizontal sweeps, where Z and Y were constant, were carried out, as represented in Figure

7. Table 2 lists the parameters used for the different test conditions. The coordinates which identify the helicopter model position refer to the centre of the rotor disk.

Before the tests involving the obstacle (T1-4), a reference Test T0 was carried out in order to assess the ground effect behaviour of the helicopter model in absence of the obstacle.

All the tests were carried out in both the wind-off and wind-on configuration. In particular, a wind velocity corresponding to an advance ratio $\mu = U_\infty/(\Omega R) = 0.05$ was adopted, in order to simulate the effect of a moderate wind that flows past the obstacle. This corresponds to a wind velocity of approximately 36 km/h for a full-scale scenario, considering that for real helicopters M_{TIP} is usually around 0.6.

Three runs were carried out for each measurement point, and the obtained results were averaged. The results for test T1 in windy condition were averaged over just two repetitions, owing to the fact that one of the runs was discarded at a later stage, after a final general data check which highlighted a system malfunctioning during this run. For every run, the motor was started from rest and then stopped again at the end of the acquisition. The acquisition took place over 5 s following a 10 s flow stabilisation. The balance zeroes were acquired immediately before and after each run and the mean of these two readings was used, even though the zero drift was quite small thanks to the short run time. The rotational speed was set equal to 2580 RPM, and maximum drifts of the order of 1% occurred during the tests. The actual RPM value was continuously acquired so that the thrust and torque coefficients would be correctly computed.

3. Results

As previously stated in section 2.1, all the test in windy conditions were carried out in the large test section of wind tunnel of Politecnico di Milano, which is 13.84 m wide, 3.84 m high and 38 m long. This test chamber is equipped with several devices allowing to produce different velocity profiles as well as different turbulence intensity and distribution. For the present activity, as no specific real conditions of a specific real site were considered, it was decided to keep the clean flow of the empty chamber, without any upstream turbolator. This flow is characterised by a floor boundary layer thickness of 0.18 cm (40% of the obstacle

Test name	Obstacle	Sweep direction	X/R	Y/R	Z/R	First point	Last point	No. of points	μ
T0	NO	Z	0	0	-	$Z/R = 1$	$Z/R = 4$	10	0 / 0.05
T1	YES	Z	-1.07	0	-	$Z/R = 2$	$Z/R = 4$	7	0 / 0.05
T2	YES	X	-	0	2	$X/R = -1$	$X/R = 1$	5	0 / 0.05
T3	YES	Z	2	0	-	$Z/R = 1$	$Z/R = 4.2$	9	0 / 0.05
T4	YES	Z	2	-1.33	-	$Z/R = 1$	$Z/R = 4.2$	9	0 / 0.05

Table 2: Test Points. (X, Y, Z) represent the position of the rotor centre with respect to the obstacle.

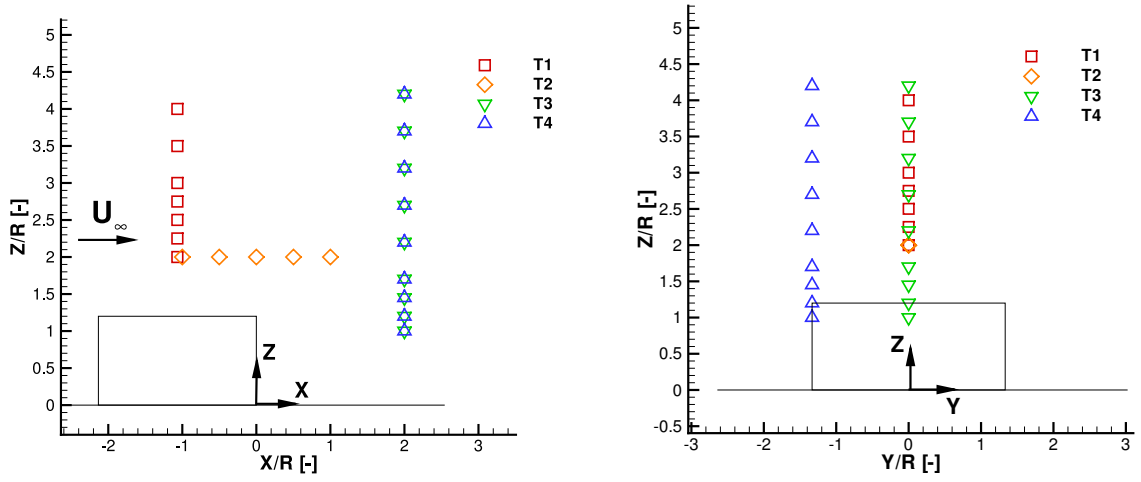

(a) Test points - Lateral View

(b) Test points - Frontal View

Figure 7: Schematic of the Test Points - Each marker corresponds to the position of the rotor centre in that test.

height) and a mean turbulence level in the order of 2%. For further information about the features of the flow inside the test section, refer to [24].

The results for the helicopter-obstacle interaction test in presence of wind ($\mu = 0.05$) will be now presented compared with those obtained for the wind-off case ($\mu = 0$). The load measurements are presented in Figures 8-13. Error bars are reported as well, and their amplitude is set to twice the estimated uncertainty, corresponding to a confidence interval of 95 %. Error bars are not presented for the in-plane moments due to the small value of its uncertainty with respect to the plot scale.

3.1. Reference results in absence of the obstacle

Let us firstly consider the test at $Z/R = 4$ in absence of the obstacle, corresponding to the out-of-ground-effect OGE condition. The comparison between the load measurements at $Z/R = 4$ for the wind-on ($\mu = 0.05$) and wind-off ($\mu = 0$) tests is presented in Table 3.

	$\mu = 0$	$\mu = 0.05$
$c_{T,OGE}$	$7.27 \cdot 10^{-3}$	$7.54 \cdot 10^{-3}$
$c_{Q,OGE}$	$7.8 \cdot 10^{-4}$	$7.63 \cdot 10^{-4}$
FM_{OGE}	0.561	0.606
$c_{Mx,OGE}/c_{Q,OGE}$	0.008	-0.14
$c_{My,OGE}/c_{Q,OGE}$	- 0.003	1.17

Table 3: Thrust coefficient, torque coefficient, moment coefficients and figure of merit at $Z/R = 4$ without the obstacle: wind-off ($\mu = 0$) and wind-on tests($\mu = 0.05$).

For the sake of full disclosure, a small difference in wind-off thrust value was found with respect to what has already been presented, for the same helicopter model, in [14]. The differences were rather small (less than 3% of the absolute value) and they practically vanish when the results are presented in terms of ratio. This discrepancy could be mainly explained by the difference in the test environments between the two test campaigns, that might have influenced, even slightly, the rotor performance in the former test. In facts

the present tests were conducted in a very large test section, where the influence of the surroundings could be considered negligible, while in the previous experiment the tests were carried out in a more confined laboratory environment outside the wind tunnel test chamber.

Coming back to the present results, a 4% thrust increase with respect to the wind-off case can be noticed (as already observed in [12]), which is caused by both the reduction of the induced velocity in advanced flight and the combination of the wind speed with the rotational velocity of the advancing and retreating blade. Since the effect on the thrust is quadratic, the thrust increase on the advancing blade is greater with respect to the decrease on the retreating one, thus creating a thrust surplus. A contextual 2% torque contraction is also present, due to the well-known decrease of the induced power in forward flight (see Glauert, [25]). A small rise in the rotor profile drag is nevertheless presents, but its effect is usually smaller with respect to the decrease in the induced power at this moderate advance ratio. The combination of the thrust increase and the torque decrease leads to a 8% increase for the figure of merit.

The wind also produces pitching and roll moments on the rotor. In particular, a negative roll moment develops on the rotor due to the combination of the wind velocity with the blade rotational velocity. This leads to a higher thrust on the advancing blade and a lower thrust on the retreating one, thus creating a roll moment owing to the stiffness of the adopted rotor. A strong nose-up pitching moment, larger than the rotor torque, also develops on the rotor. This is mainly caused by the distribution of induced velocity in forward flight: a reduced induced-velocity is experienced in the fore part of the rotor whereas an increased induced-velocity is experienced in the aft part, see Elliot et al. [26].

From now on, all the results for the thrust coefficient and figure of merit will be presented divided by their respective wind-on and wind-off OGE values, in order to highlight the effects of the ground and obstacle through a normalisation by the corresponding free-flight values. A different approach is pursued for the rotor in-plane moments, which will be presented as the difference with their respective OGE value divided by the OGE torque coefficient, i.e. $(c_M - c_{M,OGE})/c_{Q,OGE}$. This choice was driven by the the will to isolate the effect of just the ground and the obstacle. Moreover representing the moment variation as a fraction of

the rotor OGE torque helps to identify the order of magnitude of the moments that are generated in the interaction.

The reference test (Test T0) was carried out at several rotor heights in absence of the obstacle, in order to assess the helicopter performance in ground effect. As shown in Figure 8a, a reduced ground effect can be appreciated for the wind-on case. Moreover the presence of the ground starts to affect the helicopter at $Z/R = 1.5$ in the wind-on case, whereas in the wind-off case effect starts to be appreciable at $Z/R = 3$. To sum up, the ground effect in windy conditions appears to be less intense with respect to the one without wind, and it affects the helicopter only at very low heights. The same considerations can be drawn for the figure of merit behaviour of Figure 8b. For what concerns the rotor moments of Figure 8c, both the pitch and roll moments present a negative variation with respect to the OGE condition as the helicopter is getting closer to the ground in windy conditions, as was observed in [27]. This is caused by the influence of the ground vortex that is generated in ground effect for moderate advance ratios, as was described in [27] and [28].

3.2. Results in presence of the obstacle

After the reference results in absence of the obstacle, its effect on the helicopter performance will be discussed in the present section. Test T1 represents a ground effect test at several heights above the upper surface of the obstacle, reproducing a slow vertical approach to the top of the obstacle. Figure 9 presents the comparison between wind-off and wind-on measurements for Test T1, whereas Figure 10 presents the comparison between Test T0 (ground effect over an infinite surface) and T1 (ground effect over the obstacle) in terms of thrust coefficient. In the latter plot, the results for Test T1 have a Z/R offset equal to the obstacle height ($1.2R$) in order to have a direct comparison with test T0. For the wind-off case, the ground effect experienced over the obstacle is practically equivalent to the one over an infinite surface. This can be appreciated in Figure 10a, as already shown in [14], and it can be explained by the fact that the rotor projection wholly lies on the obstacle upper surface. Ground effect is mitigated in windy conditions similarly to what happened for Test T0 without the obstacle, as testified by Figure 9a. If one compares the results of test T0 and T1

in the windy case, the thrust coefficient curves (Figure 10b) are practically superimposed, as in the wind-off case. This means that, for moderate wind speed, the upwash induced by the upstream obstacle face is not capable of changing this macroscopic behaviour. A similar behaviour to the T0 test can be recognised for the pitch and roll moments of Figure 9c as well.

Test T2 considers a set of points on a horizontal line on the symmetry plane at $Z/R = 2$, representing a slow horizontal approach to the obstacle upper surface. Let us start analysing the thrust variation of Figure 11a for the wind-off case. A gradual thrust coefficient increase can be recognised as the rotor is positioned over of the obstacle for decreasing X/R, owing to the augmented rotor projection lying on the upper surface of the obstacle. $c_T/c_{T,OGE}$ is 1.04 for the outer position $X/R = 1$, that is very similar to the one measured at the same height $Z/R = 2$ in test T0 (without the obstacle). Although the rotor wake structure will be somehow different with respect to the no-obstacle case due to its impingement upon the side of the obstacle, its effect on the thrust coefficient is almost not appreciable. This suggests that the induced velocity on the rotor disk is almost unaffected by the obstacle in this particular case, as confirmed by the LDA measurements in [16]. Moving closer to the obstacle, the rotor wake behaviour is gradually more influenced. Nevertheless, at $X/R = 0.5$, the obstacle effect on the rotor loads is still very small. This counter-intuitive result is confirmed by the measurements reported in [16] and [14].

The gradual ground effect caused by the increasing obstacle blockage underneath the rotor is mitigated in windy conditions (Figure 11a), analogously to what already observed for the ground effect without the obstacle. For the outer position $X/R = 1$ the thrust coefficient is equal to the OGE value due to the fact the ground effect starts to be appreciable only at lower heights in windy conditions.

Let us now consider the moments of Figure 11c. For the wind-off case, as highlighted in [16], a very limited moment variation is encountered – below 5% of the rotor OGE torque – as the helicopter is moved over the obstacle. This does not occur anymore for $\mu = 0.05$, where the pitch moment undergoes a strong negative nose-down variation – more than 40% of the rotor OGE torque – as the helicopter is moved above the obstacle. This increase of

the nose-down pitch moment is probably due to the presence of a recirculation region above the obstacle upper surface originated by both the rotor wake and the flow separation at the obstacle windward edge.

The load results for Test 3 and 4 are shown in Figure 12. As a reminder, Test 3 and Test 4 consisted in two Z-sweeps behind the obstacle at $X/R = 2$, representing vertical landings back to the obstacle: the former at $Y/R = 0$ in the symmetry plane, the latter at $Y/R = -1.33$, behind the obstacle edge (see Figure 7b). As observed in [16], Test T3 is characterised, in absence of wind, by a severe thrust drop (up to 8 %, Figure 12a), when the helicopter is behind the obstacle due to the development of a recirculation region between the obstacle and the helicopter. This recirculation consists of the rotor wake that, after being deflected by the ground and by the vertical wall of the obstacle, is re-ingested by the rotor itself. This causes an increased induced velocity in the fore part of the rotor, together with the consequent thrust loss. Since this recirculation region mainly affects the forward part of the rotor, the inflow loses symmetry and generates a nose-down pitching moment that can be observed in Figure 12e for $Z/R < 1.5$. As the helicopter is positioned upwards, the pitching moment changes direction becoming positive, then it starts to decrease again as the influence of the obstacle becomes less intense. Comparing the outermost T2 point (at $X/R = 1$ $Z/R = 2$) and the T3 point at the closest height $Z/R = 2.2$, it can be observed that for the wind-off case, the T3 point, which is further from the obstacle presents a lower value of thrust differently from what could be expected. This can be explained by the fact that for the T2 point the flow recirculation structure producing the rotor wake re-ingestion cannot develop due to the scarce clearance between the rotor and obstacle.

The detrimental effects observed for Test T3 in the wind-off case seem to be, at least for the thrust coefficient, slightly mitigated in windy conditions (Figure 12a), probably due by the fact that external wind does not allow the complete development of such rotor wake re-ingestion. However, when the helicopter is completely behind the obstacle, i.e. $Z/R < 1.2$, a slight thrust decrease is nevertheless present. This could be explained by the fact that the wake re-ingestion is less disturbed by the external wind and, at the same time, a recirculation region is anyway present due to the obstacle wake. Considering the moment plot Figure 12e,

a very strong nose-down moment variation, of the order of magnitude of the rotor torque, is present as the helicopter is positioned downwards, behind the obstacle. This remarkable difference with respect to the OGE condition is related not only to the already mentioned recirculation, but also to the gradual reduction of the external wind effect as the helicopter enters the obstacle wake.

A completely different behaviour can be observed for test T4, where the helicopter is placed at different heights behind the obstacle lateral edge, $Y/R = -1.33$. Considering the wind-off case, Figure 13a, the detrimental effects due to the interaction with the obstacle appear to be strongly mitigated with respect to test T3, since just half of the rotor is facing the obstacle. However, in presence of wind, a severe drop in the thrust coefficient (up to 11% below the OGE value) can be appreciated for $Z/R < 1.2$ in Figure 12b, probably due to the horseshoe vortex that surrounds the obstacle (as depicted in Figure 6), further increasing the overall downwash effect on the rotor. This condition is also characterised by an even more intense nose-down variation of the pitching moment with respect to test T3, up to 1.4 times the OGE torque, as it can be appreciated in Figure 13f. The variation of the roll moment for test T4 presents an opposite trend with respect to test T3, becoming positive when the helicopter is positioned closer to the ground, Figure 13d. The difference between the two tests, at the lowest helicopter position, is up to 30% of the OGE torque. This could be explained by the fact that the advancing blade encounters lower velocities and higher downwash, being immersed in the inner wake of the obstacle.

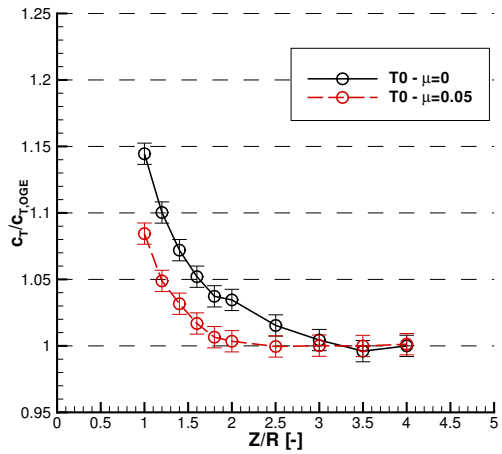

(a) Ratio between the thrust coefficient c_T and the one measured in OGE

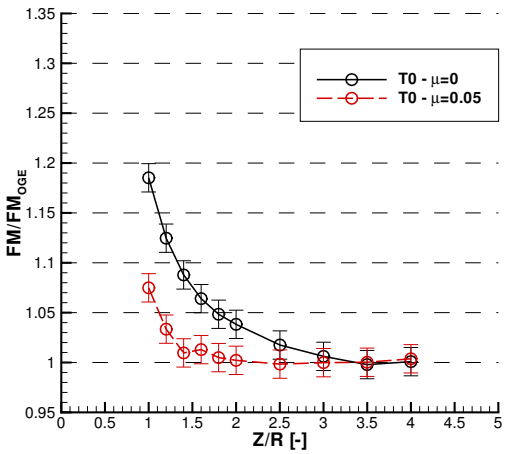

(b) Ratio between figure of merit FM and the one measured in OGE

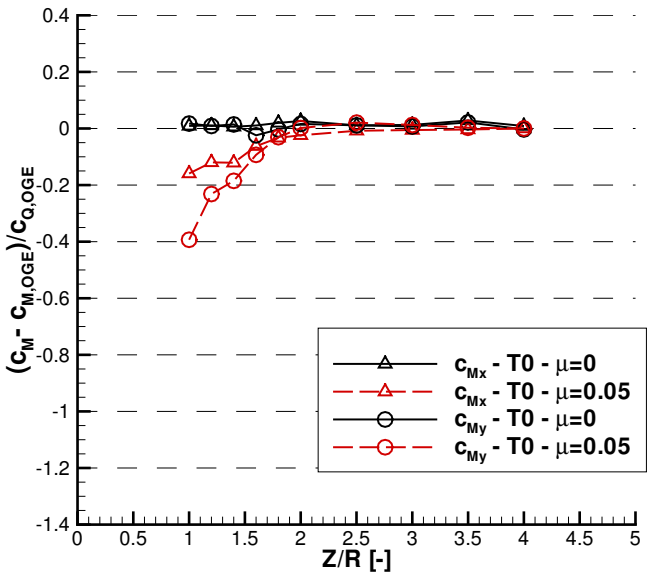

(c) Ratio between the variation of the roll/pitch moment coefficient (c_{Mx} and c_{My} respectively) and the OGE torque coefficient

Figure 8: Test T0 - Comparison between the wind-on ($\mu = 0.05$) and wind-off ($\mu = 0$) tests.

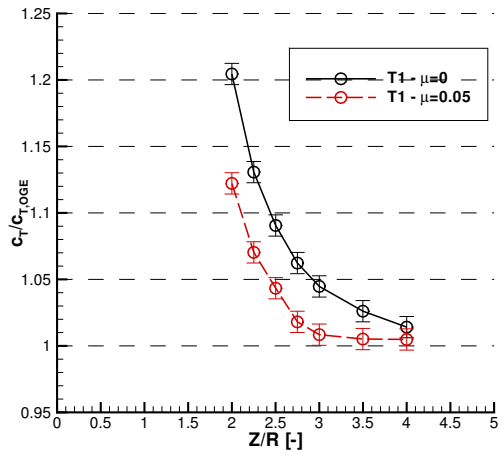

(a) Ratio between the thrust coefficient c_T and the one measured in OGE

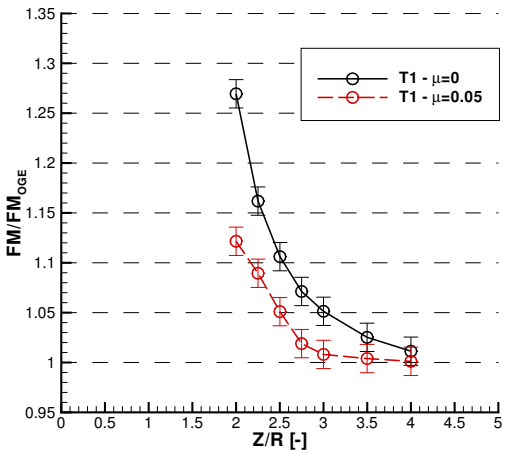

(b) Ratio between figure of merit FM and the one measured in OGE

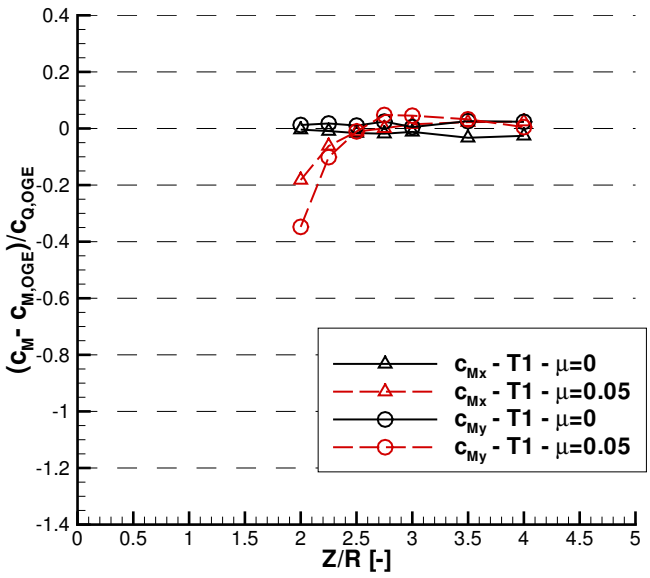

(c) Ratio between the variation of the roll/pitch moment coefficient (c_{Mx} and c_{My} respectively) and the OGE torque coefficient

Figure 9: Test T1 - Comparison between the wind-on ($\mu = 0.05$) and wind-off ($\mu = 0$) tests.

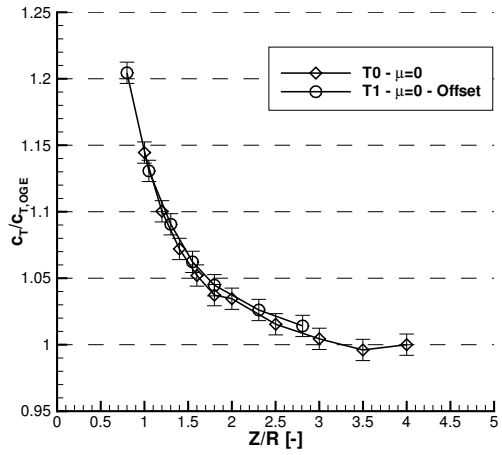

(a) Ratio between the thrust coefficient c_T and the one measured in OGE, $\mu = 0$

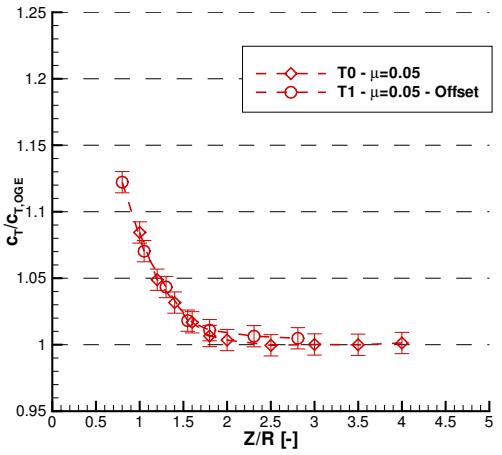

(b) Ratio between the thrust coefficient c_T and the one measured in OGE, $\mu = 0.05$

Figure 10: Comparison between Test T0 (ground effect test without obstacle) and Test T1 (ground effect on the top of the obstacle). The curve of Test T1 has a Z offset equal to the obstacle height ($1.2R$).

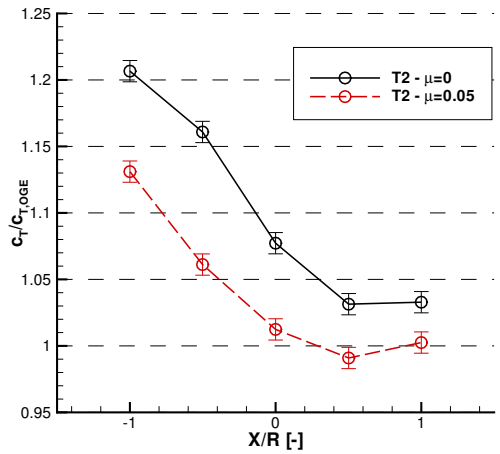

(a) Ratio between the thrust coefficient c_T and the one measured in OGE

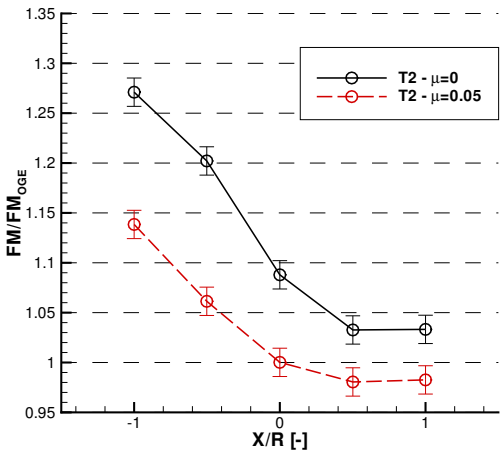

(b) Ratio between figure of merit FM and the one measured in OGE

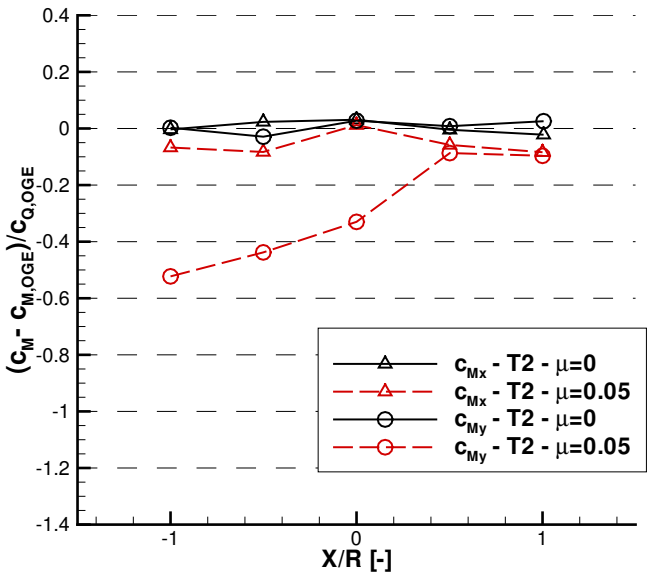

(c) Ratio between the variation of the roll/pitch moment coefficient (c_{Mx} and c_{My} respectively) and the OGE torque coefficient

Figure 11: Test T2 - comparison between the wind-on ($\mu = 0.05$) and wind-off ($\mu = 0$) tests.

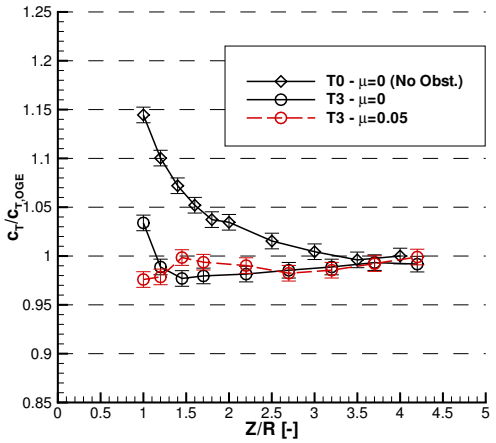

(a) T3 - Ratio between the thrust coefficient c_T and the one measured in OGE

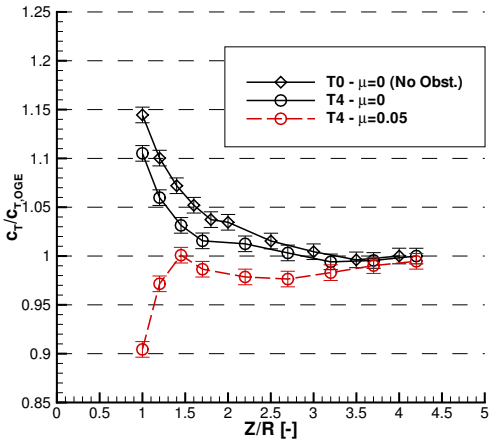

(b) T4 - Ratio between the thrust coefficient c_T and the one measured in OGE

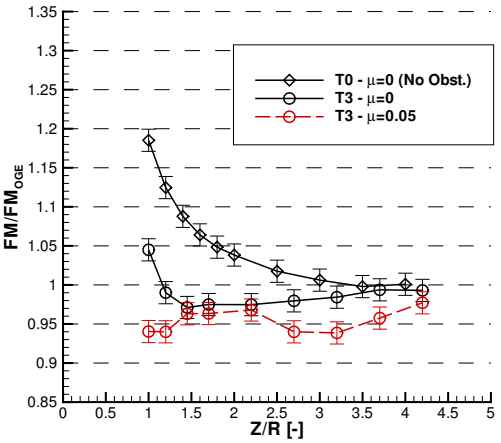

(c) T3 - Ratio between figure of merit FM and the one measured in OGE

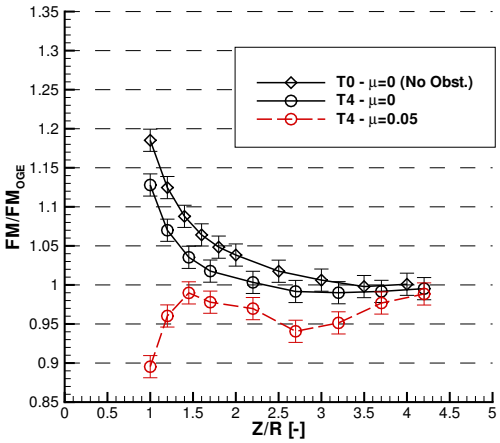

(d) T4 - Ratio between figure of merit FM and the one measured in OGE

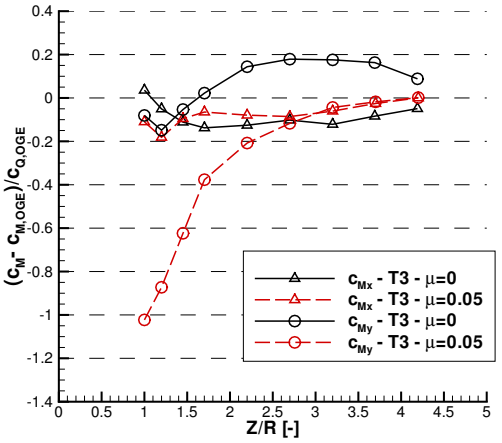

(e) T3 - Ratio between the variation of the roll/pitch moment coefficient (c_{Mx} and c_{My} respectively) and the OGE torque coefficient

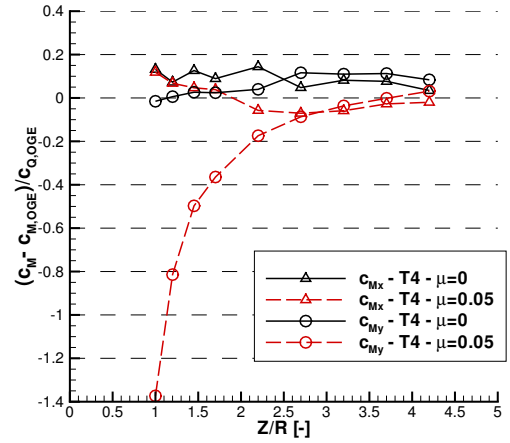

(f) T4 - Ratio between the variation of the roll/pitch moment coefficient (c_{Mx} and c_{My} respectively) and the OGE torque coefficient

Figure 12: Test T3 (left) and T4 (right) - Comparison between the wind-on ($\mu = 0.05$) and wind-off ($\mu = 0$) tests. Results of test T0 (vertical landing without obstacle) are also reported as reference.

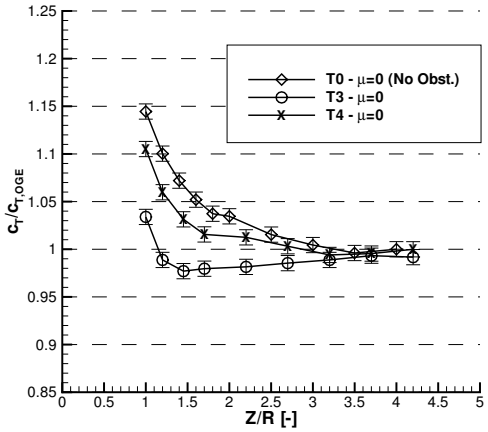

(a) Ratio between the thrust coefficient c_T and the one measured in OGE, $\mu = 0$

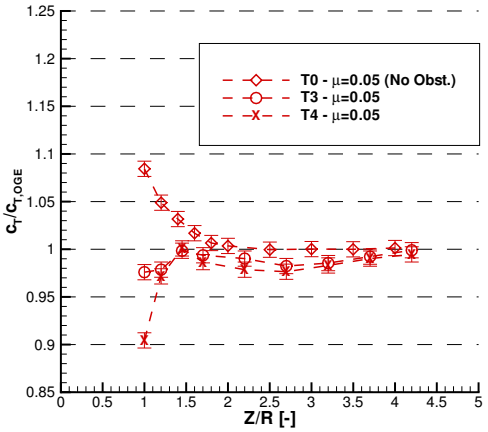

(b) Ratio between the thrust coefficient c_T and the one measured in OGE, $\mu = 0.05$

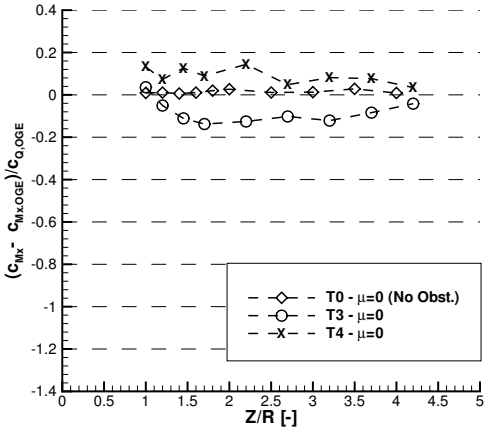

(c) Ratio between the variation of the roll moment coefficient c_{Mx} and the OGE torque coefficient, $\mu = 0$

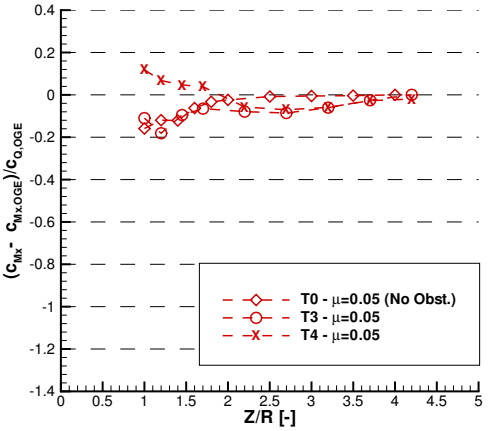

(d) Ratio between the variation of the roll moment coefficient c_{Mx} and the OGE torque coefficient, $\mu = 0.05$

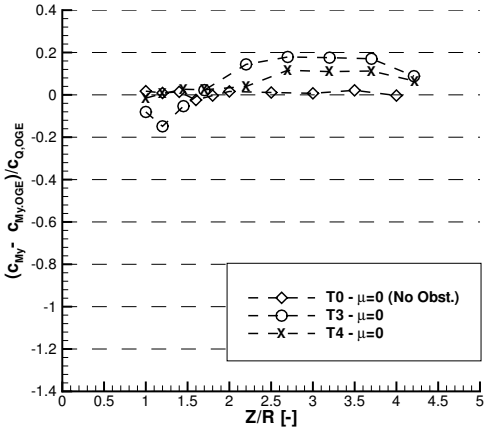

(e) Ratio between the variation of the pitch moment coefficient c_{My} and the OGE torque coefficient, $\mu = 0$

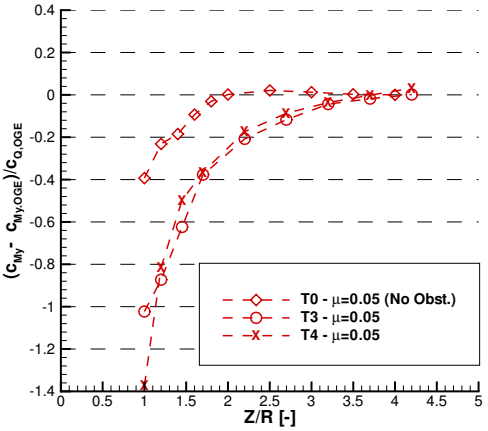

(f) Ratio between the variation of the pitch moment coefficient c_{My} and the OGE torque coefficient, $\mu = 0.05$

Figure 13: Comparison among Test T3 (vertical landing behind the obstacle at $Y/R = 0$), Test T4 (vertical landing behind the obstacle at $Y/R = -1.33$) and Test T0 (vertical landing without the obstacle).

4. Conclusions

In the present work, an experimental survey of the loads acting on the main rotor of a helicopter flying close to a low-rise cuboid obstacle in moderate windy conditions has been described. Measurements of force and moment acting on the rotor were carried out by means of a six-component balance in order to assess the rotor performance for several rotor positions with respect to the obstacle. Wind-off measurements were carried out as well in order to appreciate the effect of the wind by comparison. In general the tests highlighted remarkable effects induced by the obstacle, which has dimensions comparable to the rotor diameter, in both windy and not windy conditions. The considered moderate wind, corresponding to an advance ratio of 0.05 and thus to a velocity of 36 km/h if referred to full scale condition, was capable, despite its relatively low intensity, of affecting remarkably the essence of the phenomena generated in the helicopter-obstacle interaction. Larger effects are expected for higher advance ratios, but they have not been investigated in the present work.

The significant difference between the wind-off and the relatively low windy conditions, evokes an interactional scenario which is very complex and difficult to predict, demanding the pilot to counteract its effect on the helicopter performance. The results of the present test, carried out using a rigid rotor with fixed blade pitch, are not able to represent the real trimmed rotor condition, however they are useful for highlighting the obstacle effects that in the real flight would have to be compensated by the pilot.

A first set of measurements without the obstacle showed that the ground effect in windy conditions appears to be less intense with respect to the one without wind (the difference in the maximum achieved thrust coefficient was up to 7%), and that it affects the helicopter only very close to the ground, in particular when the rotor height is less than 1.5 radii. Moreover, similarly to what was already found in a previous work just for the wind-off case, the ground effect experienced by the helicopter over the obstacle in windy conditions is equivalent to the one over an infinite surface, thus highlighting the reduced influence of the obstacle wake during a landing on its upper surface.

The effect of the obstacle wake becomes definitely more relevant when the helicopter

model is positioned downstream of the obstacle. In particular, the detrimental effects experienced in the wind-off conditions caused by the recirculation region that develops between the rotor and the obstacle causing the wake re-ingestion seems to be slightly mitigated in windy conditions, at least for moderate helicopter heights. When the helicopter is completely behind the obstacle a slight drop in the thrust coefficient (4% of the OGE value) is nevertheless present due to the interaction with the recirculating region present in the obstacle wake. The situation can be further complicated when the helicopter is moved from the obstacle symmetry plane to the region influenced by the wake lateral structures. In particular a severe drop in the thrust coefficient (up to 11% below the OGE value) can be appreciated when the helicopter is positioned behind the obstacle lateral edge. Very strong variations in the rotor in-plane moments (up to 1.4 times the OGE torque) are also present when the helicopter enters in the obstacle wake.

References

[1] D. Lee, N. Sezer-Uzol, J. F. Horn, L. N. Long, Simulation of helicopter shipboard launch and recovery with time-accurate airwakes, Journal of Aircraft 42 (2) (2005) 448–461.

[2] G. K. Timm, Obstacle-induced flow recirculation, Journal of the American Helicopter Society 10 (4) (1965) 5–24.

[3] N. Iboshi, N. Itoga, J. Prasad, L. N. Sankar, Ground effectdd of a rotor hovering above a confined area, Frontiers in Aerospace Engineering 3 (1) (2014) 7–16.

[4] S. Zan, On aerodynamic modelling and simulation of the dynamic interface, Proceedings of the Institution of Mechanical Engineers, Part G: Journal of Aerospace Engineering 219 (5) (2005) 393–410.

[5] S. Zan, Experimental determination of rotor thrust in a ship airwake, Journal of the American Helicopter Society 47 (2) (2002) 100–108.

[6] R. G. Lee, S. J. Zan, Unsteady aerodynamic loading on a helicopter fuselage in a ship airwake, Journal of the American Helicopter Society 49 (2) (2004) 149–159.

[7] R. G. Lee, S. J. Zan, Wind tunnel testing of a helicopter fuselage and rotor in a ship airwake, Journal of the American Helicopter Society 50 (4) (2005) 326–337.

[8] C. H. Kääriä, Y. Wang, G. D. Padfield, J. S. Forrest, I. Owen, Aerodynamic loading characteristics of a model-scale helicopter in a ship's airwake, Journal of Aircraft 49 (5) (2012) 1271–1278.

[9] C. H. Kääriä, Y. Wang, M. D. White, I. Owen, An experimental technique for evaluating the aerodynamic impact of ship superstructures on helicopter operations, Ocean Engineering 61 (2013) 97–108.

[10] T. Quinliven, K. Long, Rotor performance in the wake of a large structure, in: American Helicopter Society 65th Annual Forum, Grapewine, TX, USA, 2009.

[11] G. Rajagopalan, S. Niazi, A. J. Wadcock, G. K. Yamauchi, M. J. Silva, Experimental and computational study of the interaction between a tandem-rotor helicopter and a ship, in: American Helicopter Society 61st Annual Forum, Grapewine, TX, USA, 2005.

[12] Y. Nacakli, D. Landman, Helicopter downwash/frigate airwake interaction flowfield PIV surveys in a low speed wind tunnel, in: AHS 67th annual forum, Virginia Beach, VA, USA, 2011, pp. 1–11.

[13] S. Polsky, C. Wilkinson, A computational study of outwash for a helicopter operating near a vertical face with comparison to experimental data, in: AIAA–2009–5684, AIAA Modeling and Simulation Technologies Conference, Chicago, IL, USA, 2009.

[14] G. Gibertini, D. Grassi, C. Parolini, D. Zagaglia, A. Zanotti, Experimental investigation on the aerodynamic interaction between a helicopter and ground obstacles, Proceedings of the Institution of Mechanical Engineers, Part G: Journal of Aerospace Engineering 229 (8) (2015) 1395–1406.

[15] A. Visingardi, F. D. Gregorio, T. Schwarz, M. Schmid, R. Bakker, S. Voutsinas, Q. Gallas, R. Boisard, G. Gibertini, D. Zagaglia, G. Barakos, R. Green, G. Chirico, M. Giuni, Forces on obstacles in rotor

wake - a garteur action group, 43^{rd} European Rotorcraft Forum, Milan, Italy, 2017.

[16] D. Zagaglia, M. Giuni, R. Green, Rotor-obstacle aerodynamic interaction in hovering flight: An experimental survey, in: American Helicopter Society 72^{nd} Annual Forum, West Palm Beach, FL, USA, 2016.

[17] G. Chirico, D. Szubert, L. Vigevano, G. N. Barakos, Numerical modelling of the aerodynamic interference between helicopter and ground obstacles, CEAS Aeronautical Journal 8 (4) (2017) 589–611.

[18] G. Gibertini, L. Gasparini, A. Zasso, Aerodynamic design of a civil-aeronautical low speed large wind tunnel, in: AGARD 79th Fluid Dynamics Panel Symposium, AGARD, Moscow, Russia, 1997, pp. 6.1–6.10.

[19] R. Martinuzzi, C. Tropea, The flow around surface-mounted, prismatic obstacles placed in a fully developed channel flow, Journal of Fluids Engineering 115 (1993) 85–92.

[20] H. C. Lim, T. Thomas, I. P. Castro, Flow around a cube in a turbulent boundary layer: LES and experiment, Journal of Wind Engineering and Industrial Aerodynamics 97 (2) (2009) 96–109.

[21] J. Sousa, Turbulent flow around a surface-mounted obstacle using 2D-3C DPIV, Experiments in Fluids 33 (6) (2002) 854–862.

[22] J.-Y. Hwang, K.-S. Yang, Numerical study of vortical structures around a wall-mounted cubic obstacle in channel flow, Physics of Fluids 16 (7) (2004) 2382–2394.

[23] A. Yakhot, H. Liu, N. Nikitin, Turbulent flow around a wall-mounted cube: A direct numerical simulation, International journal of heat and fluid flow 27 (6) (2006) 994–1009.

[24] A. Zasso, S. Giappino, S. Muggiasca, L. Rosa, Optimization of the boundary layer characteristics simulated at politecnico di milano boundary layer wind tunnel in a wide scale ratio ranger, in: Proceedings of the 6th Asia-Pacific Conference on Wind Engineering, Seoul, Korea., 2005.

[25] H. Glauert, On the horizontal flight of a helicopter, HM Stationery Office, 1928.

[26] J. W. Elliott, S. L. Althoff, R. H. Sailey, Inflow measurement made with a laser velocimeter on a helicopter model in forward flight. volume 1: Rectangular planform blades at an advance ratio of 0.15, NASA 100545.

[27] H. Curtiss, M. Sun, W. Putman, E. Hanker, Rotor aerodynamics in ground effect at low advance ratios, Journal of the American Helicopter Society 29 (1) (1984) 48–55.

[28] N. Nathan, R. Green, The flow around a model helicopter main rotor in ground effect, Experiments in fluids 52 (1) (2012) 151–166.